Eur. Phys. J. A **25**, 387–396 (2005)
DOI 10.1140/epja/i2005-10134-y

THE EUROPEAN PHYSICAL JOURNAL A

E2 transitions between positive- and negative-parity states of the ground-state alternating-parity bands

T.M. Shneidman[1], R.V. Jolos[1,2,a], R. Krücken[3,4], A. Aprahamian[5], D. Cline[6], J.R. Cooper[4], M. Cromaz[7], R.M. Clark[7], C. Hutter[4], A.O. Macchiavelli[7], W. Scheid[2], M.A. Stoyer[8], and C.Y. Wu[5]

[1] Joint Institute for Nuclear Research, 141980 Dubna, Russia
[2] Institut für Theoretische Physik, Justus-Liebig-Universität Giessen, Heinrich-Buff-Ring 16, D-35392 Giessen, Germany
[3] Physik Department E12, Technische Universität München, D-85747 Garching, Germany
[4] A.W. Wright Nuclear Structure Laboratory, Yale University, New Haven, CT 06520, USA
[5] Nuclear Structure Laboratory, University of Notre Dame, Notre Dame, IN 46556, USA
[6] Nuclear Structure Research Laboratory, University of Rochester, Rochester, NY 14627, USA
[7] Nuclear Science Division, Lawrence Berkeley National Laboratory, Berkeley, CA 94720, USA
[8] Lawrence Livermore National Laboratory, Livermore, CA 94551, USA

Received: 19 May 2005 / Revised version: 27 July 2005 /
Published online: 23 September 2005 –
Communicated by D. Schwalm

Abstract. Experimental transition probabilities between states of the ground-state alternating-parity bands of ^{144}Ba and their theoretical analysis are presented. Lifetimes of states in ^{144}Ba have been measured using the recoil distance method following spontaneous fission of ^{252}Cf. The experiment was performed at the Lawrence Berkeley National Laboratory employing the Gammasphere array and the New Yale Plunger Device. The experimental data show a significantly larger value of the $E2$ transition probability between the negative-parity states compared to the positive-parity ones. It is shown that this effect can be explained by a higher weight of the deformed component in the wave functions of the odd-I states. In the framework of the cluster approach it is explained by a higher weight of the alpha-cluster component in the wave function of the negative-parity states compared to the positive-parity ones. In the framework of the traditional collective model with the quadrupole and octupole degrees of freedom the same effect is explained by a higher value of the quadrupole deformation at the minima of the potential energy as a function of β_{20} and β_{30} compared to its value at the top of the barrier separating two physically equivalent minima, having opposite signs of the octupole deformation. Additionally, the dependence on parity of the $E2$ transition probability is analyzed qualitatively in nuclei with a minimum at $\beta_{30} = 0$ in the collective potential energy and compared to experimental data for ^{148}Nd.

PACS. 21.60.Ev Collective models – 21.60.Gx Cluster models – 23.20.Js Multipole matrix elements – 27.60.+j $90 \leq A \leq 149$

1 Introduction

Quadrupole and octupole modes are the most important collective degrees of freedom determining the nuclear properties at low excitation energies. For this reason an understanding of their dynamics is important for the development of the collective nuclear model. Among the problems which should be clarified is the role of the interplay of the quadrupole and octupole modes.

The observation of the low-lying negative-parity states in actinides and in heavy Ba and Ce isotopes [1,2] has shown that these nuclei have reflection asymmetric shapes or, at least, are characterized by a presence of strong reflection asymmetric correlations together with the quadru-pole ones. This fact gives the grounds to consider the rotational-like sequences of the lowest positive- and negative-parity states $0^+, 1^-, 2^+, 3^-, \ldots$ as a unified ground-state alternating-parity band. The formation of the rotational bands is connected in general with a constant quadrupole deformation, while the lowering of the negative-parity states is a signature of the reflection asymmetric deformation. Therefore, the investigation of the properties of the alternating-parity bands should include both quadrupole and reflection asymmetric degrees of freedom and their interplay.

One of the well-known characteristics of the alternating-parity bands is the parity splitting which is a shift up in energy of the negative-parity states with respect to

[a] e-mail: jolos@thsun1.jinr.ru

the positive-parity ones. This phenomenon is seen as the $\Delta I = 1$ staggering in the excitation energies. This parity splitting effect is explained [3–5] by an angular-momentum dependence of the penetration probability through the barrier separating two minima in the potential energy as a function of the quadrupole and the reflection asymmetric collective coordinates. The octupole deformation parameter β_{30} or the cluster degree of freedom [6,4] can be used as the latter one. The height of the barrier increases with angular momentum because the moment of inertia is larger at the minimum compared to its value at the barrier top. Since the moment of inertia is also a function of the quadrupole deformation coordinate, correlations between the quadrupole and reflection asymmetric degrees of freedom are expected [7]. Indeed, for such nuclei the motion of the system in the $\beta_{20}\beta_{30}$-plane is correlated as a softer mode, which describes a motion along the valley connecting the minimum with the barrier top, and a more rigid mode describing fluctuations around this trajectory are formed. The softer mode is just the cluster mode used in [4,5].

The other indication for the presence of the quadrupole – reflection asymmetry correlations is an enhanced $E2$ transition probability between the negative-parity states in the ground-state alternating-parity band of ^{144}Ba. Experimental evidence for this enhanced quadrupole moment is presented in this work. Preliminary results have been presented in [8], which is consistent with the results recently reported in ref. [9].

The model which is based on correlations between the quadrupole and reflection asymmetric degrees of freedom and which was already applied to the description of the properties of alternating-parity bands has been developed in [4,5]. In this model a collective motion of a nuclear shape is considered, which leads with some probability to the formation of a cluster-type shape. The only collective degree of freedom considered in this model describes a mass asymmetry of the cluster configuration. Quadrupole and octupole deformations are functions of this cluster degree of freedom [10] and they both evolve with the cluster degree of freedom. It was shown that this model provides an explanation of the variation from nucleus to nucleus of the observed value of the parity splitting for different values of the angular momentum. This means that the model describes correctly a variation of the potential energy as a function of the reflection asymmetric coordinate and angular momentum I for many considered nuclei.

The aim of the present paper is to present the results of the measurements of the $E2$ transition probabilities in the ground-state alternating-parity band of ^{144}Ba, which can be considered as a nucleus with a strong reflection asymmetric correlations or permanent octupole deformation, and to analyze the electromagnetic transitions between the states of this band. There will be an emphasis on the description of the $E2$ transitions based mainly on the cluster model approach and partly on the other existing theoretical models. In this connection it is important to mention that the threshold energy for the decay of ^{144}Ba into ^{140}Xe + ^{4}He is only 1.2 MeV above the ground-state energy of ^{144}Ba. This indicates a possible importance of the α-cluster component in the wave function of the low-lying states of ^{144}Ba.

To stress a contrast in the mechanisms determining parity dependence of the $E2$ transition probabilities in nuclei, having permanent octupole deformation or being near to be octupole deformed, and octupole vibrational nuclei, we consider in sect. 4 a model describing octupole vibrations in quadrupole deformed nuclei. This model is applied to the description of the $E2$ transitions between the low-lying negative-parity states in ^{148}Nd which is an octupole vibrational nucleus.

2 Experimental data

Lifetimes of excited states in ^{144}Ba were measured following the spontaneous fission of ^{252}Cf. The experiment was performed at the Lawrence Berkeley National Laboratory by employing the New Yale Plunger Device (NYPD) [11] and a photocell array in conjunction with the Gammasphere array [12], which comprised 100 Compton-suppressed high-volume Ge detectors. A schematic of the experiment can be found in ref. [13]. Fragments originating from a thin $\sim$ 70 μCi ^{252}Cf source on a stretched ~ 1 mg/cm^2 Ni foil were detected by a set of photocells, which covered an angular range of $\pm$ 20° with respect to the plunger axis. The complementary fragments, after being somewhat slowed in the Ni foil, traveled a variable distance before being stopped in a stretched 10 mg/cm^2 Au stopper foil. Coincidence events were recorded if at least three suppressed gamma rays were detected in the Ge detectors and one particle in the photocell array within a time window of about 200 ns. A gate on the fragment energy allowed selection of the lower ($A \sim 100$) and higher ($A \sim 140$) mass fission products, respectively.

Approximately 85×10^6 coincidence events were collected at each of the 22 source-to-stopper distances between 9 and 7000 μm for approximately one day per distance. The data were stored in an energy sorted list-mode database, using the software package Blue [14]. By applying gating conditions on particle energy, gamma-ray energy and time-gated spectra were generated for each distance and intervals of 0.1 width in $\cos\theta$ [0.0–0.1, 0.1–0.2, 0.2–0.3, ...], where θ is the angle between the emitted γ-ray and the direction of the emitting fission fragment. Gates were placed on Doppler-shifted energies for transitions above the level of interest and both shifted and unshifted transition energies below the level of interest. Figure 1 shows background subtracted spectra gated on the ground-state transition ^{144}Ba in order to show several transitions of interest.

The data was analyzed using the differential decay curve method [15] which, for this experiment, has been already been described in more detail in ref. [13]. In compact form, the lifetime can be extracted from the intensities of the shifted and unshifted peaks at different distances using a simple ratio of intensities and their derivatives, respectively. If the level of interest is populated by transition B

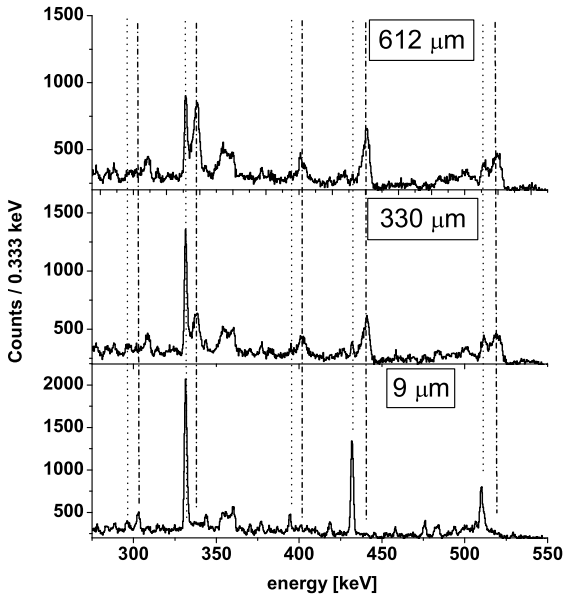

Fig. 1. Background subtracted single-gated spectra on the ^{144}Ba ground-state transition at source-to-stopper distances of 9, 330, and 612 μm for angles $\theta < 46^\circ$ between the emitted γ-rays and the emitting fission fragment. In the spectra, unshifted (dotted lines) and Doppler-shifted (dash-dotted lines) components of the 302 keV $9^- \rightarrow 7^-$, 331 keV $4^+ \rightarrow 2^+$, 394 keV $7^- \rightarrow 6^+$, and 431 keV $6^+ \rightarrow 4^+$ transitions in ^{144}Ba are indicated.

and depopulated by transition A, and $I^{A,B}_{u,s}$ are the unshifted (u) and shifted (s) intensities of transitions A and B, respectively, then the lifetime is given by

$$\tau(x) = \frac{F(x)}{G(x)} \equiv \frac{I^A_u(x) - \frac{I^A_u(x)+I^A_s(x)}{I^B_u(x)+I^B_s(x)} \cdot I^B_u(x)}{v\frac{\mathrm{d}}{\mathrm{d}x} I^A_s(x)} \quad . \qquad (1)$$

Here, v is the velocity projection of the fission fragment on the plunger axis. If the shifted component of the direct feeder transition is used as a gate, then the unshifted component $I^B_u(x) = 0$ for all source-to-stopper distances x, and the lifetime can be found only by the intensities of the unshifted peaks and the derivative of the intensities of the shifted peaks, $\tau(x) = \left(I^A_u(x)\right) / \left(v\frac{\mathrm{d}}{\mathrm{d}x} I^A_s(x)\right)$, as shown in fig. 2 for the 394 keV $7^- \rightarrow 6^+$ transition in ^{144}Ba. Doubly gated spectra using coincidences between transitions feeding the 7^- level and transitions in the decay of this level were used in this analysis.

Lifetimes have been obtained for the $4_1{}^+$ and $6_1{}^+$ levels of the ground-state band and the 7^- level of the octupole band in ^{144}Ba. The results are summarized in table 1. Preliminary results for ^{144}Ba have been published in [8].

While the decay of the 9^- state is visible in the spectra shown in fig. 1, it was impossible to perform a DDCM analysis in coincidence mode for this state. Single-gated spectra on direct or indirect feeding transitions of the 9^- state were not sufficiently clean for a reliable analysis. In particular, the proximity of the 506 keV $11^- \rightarrow 9^-$ transition to the much more intense 509 keV $8^+ \rightarrow 6^+$ transition poses the main problem. In double-gated spectra for the $9^- \rightarrow 7^-$ transition, the obtained statistics transitions feeding the 9^- state were insufficient for a reliable analysis. Therefore, we were unable to extract a lifetime for this state.

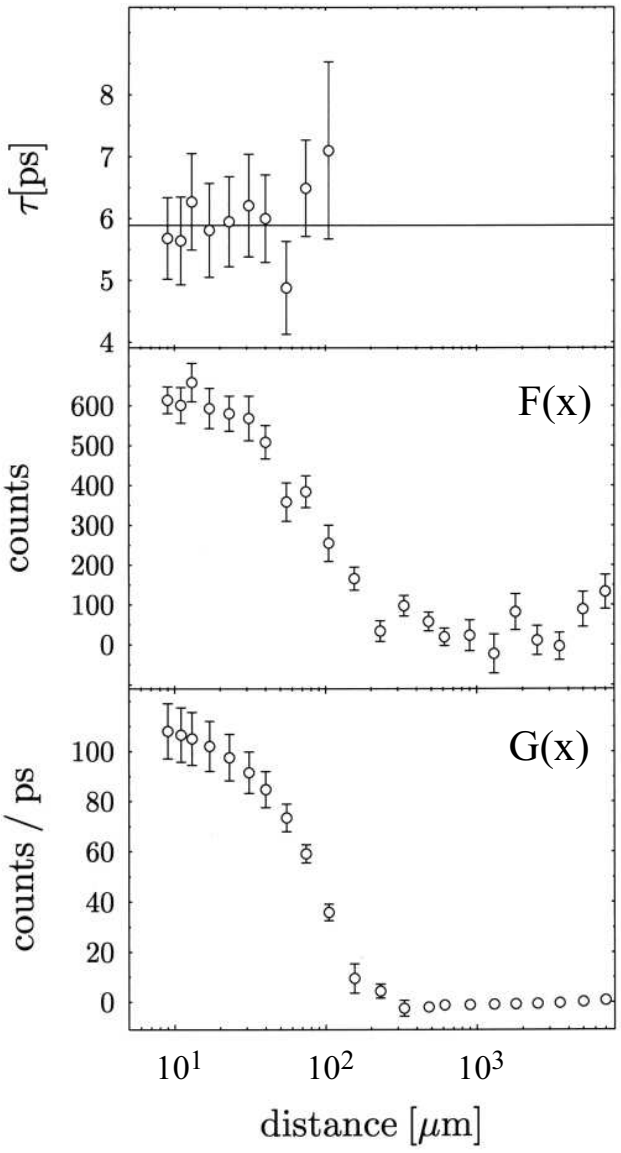

Fig. 2. The functions $F(x)$ and $G(x)$ in eq. (1) as well as the lifetime values $\tau(x)$ as functions of the source-to-stopper distance for the $7^- \rightarrow 6^+$ transition in ^{144}Ba. Only statistical errors are given in this picture. For a discussion of the treatment of systematic uncertainties, see ref. [13].

3 Model consideration of the E2 transitions between the negative-parity states in ^{144}Ba

In our approach to describe the properties of the alternating-parity bands the mass asymmetry coordinate

Table 1. Lifetimes, $B(E\lambda)$ values, transition quadrupole moments Q_t for $E2$ transitions and dipole moment D_t for the $E1$ transition obtained in the present work for ^{144}Ba.

$I_i^\pi \to I_f^\pi$	E_γ (keV)	$E\lambda$	τ (ps)	$B(E\lambda)$ (e^2 fm$^{2\lambda}$)	Q_t (e fm^2)	D_t (e fm)
$4^+ \to 2^+$	331	$E2$	74 (4)	2700 (150)	308 (9)	
$6^+ \to 4^+$	431	$E2$	21 (2)	2590 (250)	287 (14)	
$7^- \to 5^-$	317	$E2$	5.7 (10)	8000 (1800)	500 (60)[a]	
$7^- \to 6^+$	394	$E1$		1.5 (3)$\cdot 10^{-3}$		0.12 (1)[a]

[a] Using branching ratios of 1.00(6) and 0.22 (3) for the 394 and 317 keV transitions [16].

$\eta = (A_1 - A_2)/(A_1 + A_2)$ ($\eta = 1$ if $A_1 = A, A_2 = 0$) is used as a relevant collective variable instead of the parametrization of the nuclear shape in terms of the quadrupole and octupole deformation parameters. Here A_i is a mass number of the i-th cluster. Since η is a dynamical variable, the ground-state wave function can be a superposition of different cluster configurations which contribute with certain probabilities. A relative contribution of each cluster component in the total wave function is determined by the potential energy of the collective Hamiltonian described below and the inertia coefficient. Our calculations for actinides and heavy Ba and Ce isotopes have shown that in the considered cases configuration $^{(A-4)}(Z-2) + {}^4$He with the alpha cluster has the potential energy which is close to or even smaller than the energy of the mononucleus ($|\eta| = 1$). The weight of the alpha-cluster component in the ground-state wave function of nuclei with strong reflection asymmetric correlations is of the order of (2–5)%. However, it increases with angular momentum and is larger for the negative-parity states compared to the positive-parity ones. Since the energies of the configurations with a light cluster heavier than an alpha cluster increase rapidly with decreasing $|\eta|$, we can restrict our consideration to configurations with the light clusters not heavier than Li, *i.e.* by configurations near $|\eta| = 1$. For this reason it is convenient to introduce the collective variable x which is related to η in the following way:

$$\begin{aligned} x &= -\eta + 1 \quad \text{if} \quad \eta > 0\,, \\ x &= -\eta - 1 \quad \text{if} \quad \eta \le 0\,. \end{aligned} \tag{2}$$

The Hamiltonian describing a motion in x has the form

$$H = -\frac{\hbar^2}{2B_\eta}\frac{\mathrm{d}^2}{\mathrm{d}x^2} + U(x, I), \tag{3}$$

where B_η is a constant effective inertia parameter and $U(x, I)$ is a potential energy. The potential energy of a system is given as

$$U(x, I) = B_1(x) + B_2(x) + V(x, I), \tag{4}$$

where $B_1(x)$ and $B_2(x)$ are the experimental binding energies of the heavy and the light clusters at the given mass asymmetry x. The quantity $V(x, I)$ is a nucleus-nucleus potential given as

$$V(x, I) = V_{\mathrm{Coul}}(x, I) + V_{\mathrm{rot}}(x, I) + V_N(x) \tag{5}$$

with the Coulomb V_{Coul}, centrifugal $V_{\mathrm{rot}} = \hbar^2 I(I+1)/2\Im$ and the nuclear interaction V_N potentials. The nuclear interaction potential has a double folding form with the ground-state nuclear densities. Antisymmetrization between nucleons belonging to different clusters is imitated by a density dependence of the nucleon-nucleon forces which are responsible for the repulsive core in the cluster-cluster interaction potential. Details of the calculation of V_N are given in [17]. The parameters of the nucleon-nucleon interaction are fixed in the nuclear-structure calculations [18]. The specific point in the calculations of the potential energy is $x = 0$. Since the ground-state wave function is distributed in x, the potential energy at $x = 0$ is fixed so as to reproduce the experimental binding energy of the $^A Z$ nucleus with respect to $U(x_\alpha)$, where x_α corresponds to the α-cluster configuration.

Thus, the potential $U(x, I)$ of the Hamiltonian (3) contains no free parameters. It depends on the binding energies of the clusters which are taken from the experimental data. The method of calculation of the inertia coefficient B_η is given in [19]. Our calculations show that B_η is a smooth function of the atomic mass number. As a consequence, in our previous calculations [4] we have taken the same value of B_η for nuclei belonging to the same mass region. For instance, for all actinides we have taken $B_\eta = 20 \cdot 10^4 m_0 \cdot \mathrm{fm}^2$, where m_0 is the nucleon mass. The approach described above has been succsessfully applied in [4] to the description of the energy spectra and the transitional dipole, quadrupole and octupole moments for the experimentally measured transitions for the chains of the Pu, U, Th and Ra isotopes.

We parameterize the moment of inertia of the cluster configurations by

$$\Im(x) = 0.85\left(\Im_{1,\mathrm{rigid}} + \Im_{2,\mathrm{rigid}} + m\frac{A_1 A_2}{A}R_m^2\right), \tag{6}$$

where $\Im_{i,\mathrm{rigid}}$ is the rigid-body moment of inertia of the i-th cluster, m is the nucleon mass, R_m is the distance between centers of mass of two clusters and the coefficient 0.85 was taken because it is known [20] that the moments of inertia of the superdeformed state are about 85% of the rigid-body limit. As was shown in [10], the highly deformed states are well described as cluster systems. The moment of inertia of the mononucleus $\Im(x = 0)$ is

Table 2. Experimental ($E_{\rm exp}$) and calculated ($E_{\rm calc}$) energies of states of the alternating-parity band in ^{144}Ba. Energies are given in keV. Experimental data are taken from [21].

I^π	$E_{\rm exp}$	$E_{\rm calc}$
0^+	0	0
1^-	759	701
2^+	199	178
3^-	838	863
4^+	530	559
5^-	1039	1127
6^+	962	1052
7^-	1355	1461
8^+	1471	1546
9^-	1773	1847
10^+	2044	2018
11^-	2279	2281
12^+	2667	2500
13^-	2864	2764
14^+	3321	3019
15^-	3519	3301

Table 3. Transitional electric dipole moment for transitions in ^{144}Ba.

$I_{\rm i}^\pi \to I_{\rm f}^\pi$	$D_{0({\rm theor})}$ (e fm)	$D_{0({\rm exp})}$ (e fm)
$0^+ \to 1^-$	0.045	–
$1^- \to 2^+$	0.051	–
$2^+ \to 3^-$	0.054	–
$3^- \to 4^+$	0.072	–
$4^+ \to 5^-$	0.080	–
$5^- \to 6^+$	0.112	–
$6^+ \to 7^-$	0.122	0.12(1)[a]; 0.17(3)[b]
$7^- \to 8^+$	0.159	–
$8^+ \to 9^-$	0.171	–
$9^- \to 10^+$	0.195	–
$10^+ \to 11^-$	0.206	–
$11^- \to 12^+$	0.222	–
$12^+ \to 13^-$	0.230	–
$13^- \to 14^+$	0.240	–
$14^+ \to 15^-$	0.246	–

([a]) This work.
([b]) Reference [9].

fixed so as to reproduce the experimental energy of the first 2^+ state.

The potential U and the moment of inertia $\Im$ are calculated for special cluster configurations only, namely, for the mononucleus and for the cluster configurations with the α and Li clusters as light clusters. These calculated points are used then to interpolate the potential and the moment of inertia smoothly by polynomials.

Solving the eigenvalue problem with the Hamiltonian (3) we obtain the energies and the wave functions $\phi_I(x)$ for every value of I. The wave functions are used then to calculate the reduced transition probabilities. The eigenfunctions of the Hamiltonian (3) have a well-defined parity with respect to the $x \to -x$ reflection which is equivalent to the spatial reflection [4].

Table 4. Transitional electric quadrupole moment for transitions in ^{144}Ba.

$I_{\rm i}^\pi \to I_{\rm f}^\pi$	$Q_{2({\rm theor})}$ (e fm^2)	$Q_{2({\rm exp})}$ (e fm^2)
$0^+ \to 2^+$	338	325(9)[b]; 338 (12)[c]
$1^\to - 3^-$	417	–
$2^+ \to 4^+$	347	308(9)[a]; 379(27)[d]; 330(16)[c]
$3^- \to 5^-$	425	–
$4^+ \to 6^+$	366	287(14)[a]; 283(16)[c]; 247(27)[d]
$5^- \to 7^-$	436	499(55)[a]; 730 (140)[c]
$6^+ \to 8^+$	399	266(20)[c]
$7^- \to 9^-$	447	230(37)[c]
$8^+ \to 10^+$	433	–
$9^- \to 11^-$	456	–
$10^+ \to 12^+$	453	–
$11^- \to 13^-$	463	–
$12^+ \to 14^+$	463	–
$13^- \to 15^-$	458	–

([a]) This work.
([b]) Reference [22].
([c]) Reference [9].
([d]) Reference [23].

Table 5. Transitional electric octupole moment for transitions in ^{144}Ba.

$I_{\rm i}^\pi \to I_{\rm f}^\pi$	Q_3 (e fm^3)
$0^+ \to 3^-$	1409
$1^- \to 4^+$	1708
$2^+ \to 5^-$	1508
$3^- \to 6^+$	2066
$4^+ \to 7^-$	1768
$5^- \to 8^+$	2418
$6^+ \to 9^-$	2189
$7^- \to 10^+$	2657
$8^+ \to 11^-$	2582
$9^- \to 12^+$	2811
$10^+ \to 13^-$	2810
$11^- \to 14^+$	2913
$12^+ \to 15^-$	2931

With the obtained wave functions we have calculated the reduced matrix elements of the electric transition multipole moments $Q_t(E\lambda)$ with $\lambda = 1$, 2 and 3 for the ground-state alternating-parity band. The quadrupole transition operator in this model is given by the expression

$$Q_{2\mu} = \sqrt{\frac{5}{16\pi}} D^2_{\mu 0} Q_{20}(x)\,, \tag{7}$$

where $Q_{20}(x)$ is the intrinsic quadrupole moment for the given value of the reflection asymmetry coordinate x determined above. For the reduced $E2$ transition matrix element we obtain

$$\langle I \parallel Q_2 \parallel I-2\rangle = \sqrt{\frac{5}{16\pi}}\sqrt{2I-3}C^{I0}_{I-2020} \times \int \phi_I(x) Q_{20}(x) \phi_{I-2}(x)\,. \tag{8}$$

Table 6. Angular-momentum dependence of the calculated $B(E1; I \to I-1)$ in units of $B(E1)_W = 1.73\ e^2 \cdot \mathrm{fm}^2$ and the branching ratio $B(E1; I \to I-1)/B(E2; I \to I-2)$ for ^{144}Ba. For comparison, the experimental data taken from [16] are presented in the column "exp".

I^π	$B(E1; I \to I-1)/B(E1)_W$ (10^{-3}) calc	$B(E1; I \to I-1)/B(E2; I \to I-2)$ $(10^{-6} \cdot \mathrm{fm}^{-2})$ calc	exp
7^-	0.94	0.27	0.18(3)
8^+	1.64	0.54	1.02 (6)
9^-	1.91	0.50	0.58 (7)
10^+	2.50	0.68	0.83 (12)
11^-	2.79	0.68	0.73 (13)
12^+	3.26	0.81	0.86 (22)
13^-	3.49	0.81	1.10 (30)
14^+	3.85	0.90	0.55 (17)
15^-	4.05	0.94	1.15 (43)

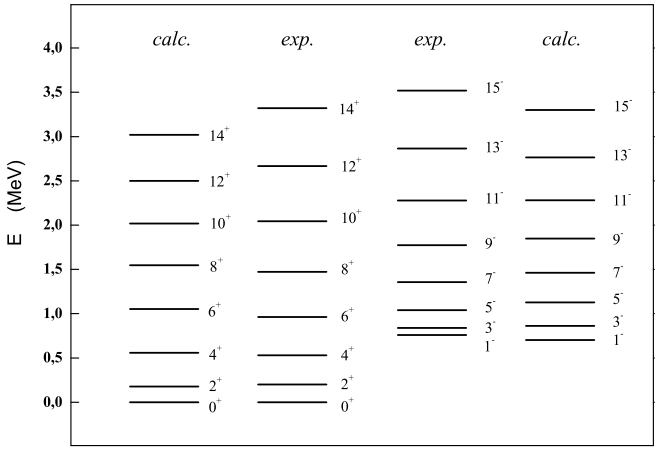

Fig. 3. Experimental and calculated spectra of the ground-state alternating-parity band of ^{144}Ba. The experimental data are taken from [21].

The wave functions $\phi_I(x)$ of the negative-parity states are concentrated farther from $x = 0$ than the wave functions of the positive-parity states. The intrinsic quadrupole moment $Q_{20}(x)$ increases with increasing $|x|$ since the cluster configurations are more deformed than the mononucleus. For this reason the $E2$ transition matrix elements are larger for the negative-parity states in nuclei with permanent octupole deformation.

The effective charge for the $E1$ transition has been taken to be equal to $e(1 + \chi)$ with the average state independent value $\chi = -0.7$. In the case of $E2$ transitions we did not renormalize the charge. For the octupole transitions our model includes only the octupole mode responsible for the shape variation and deformation of the nuclear surface. However, high-frequency isovector as well as isoscalar octupole modes are not included in the model Hamiltonian. Their combined effect leads to a renormalization of the effective octupole charge $\delta e_3^{(\mathrm{pol})} = (0.5 + 0.3\tau_z)e$ [24], *i.e.* $e^{(\mathrm{eff})}_{3,\mathrm{proton}} = 1.2e$ for protons and $e^{(\mathrm{eff})}_{3,\mathrm{neutron}} = 0.8e$ for neutrons.

The results of our calculations for ^{144}Ba of the excitation energies and the $Q_t(E\lambda)$ are shown in tables 2–6 and in figs. 3–5 in comparison to available experimental data. The calculated ground-state wave function has its maximum in the vicinity of $x = 0$. The results obtained are in good agreement with the existing experimental data. Figure 4 and table 4 illustrate an angular-momentum dependence of the intrinsic transition quadrupole moment.

In table 6 are presented the results of calculations of the absolute values of $B(E1; I \to I-1)$ and of the branching ratios $B(E1; I \to I-1)/B(E2; I \to I-2)$. They are compared with the experimental data from [16]. The comparison shows that, taking the experimental error bars into account, this is not a bad agreement, besides the 8^+ and 14^+ states.

In the framework of the cluster approach a larger value of the $E2$ transitional moment for the negative-parity states is explained by a higher weight of the alpha-cluster component in the wave function of the odd-I states which is zero at the barrier top because of its asymmetry with respect to the $x \to -x$ reflection. The alpha-cluster configuration has larger quadrupole and octupole deformations than the mononucleus one. This explanation has its counterpart in the model with the quadrupole and octupole collective modes conserving axial symmetry. The effect of an increase of $B(E2; I+2 \to I)$ for the transitions between the negative-parity states compared to the positive-parity ones is explained in the following way [7] for this model. The potential energy as a function of β_{20} and β_{30} has two minima located at $\beta_{20} = (\beta_{20})_{\min} \neq 0$ and $\beta_{30} = \pm(\beta_{30})_{\min} \neq 0$. Both minima are physically equivalent. They are transformed one into another by a reflection in a plane perpendicular to the axial symmetry axis. If the barrier separating these minima is not high enough, the system can be found with nonzero probability at the top of the barrier. If the barrier is located at $(\beta_{20})_{\mathrm{barrier}}$ which is smaller than $(\beta_{20})_{\min}$ ($(\beta_{30})_{\mathrm{barrier}} = 0$ by definition),

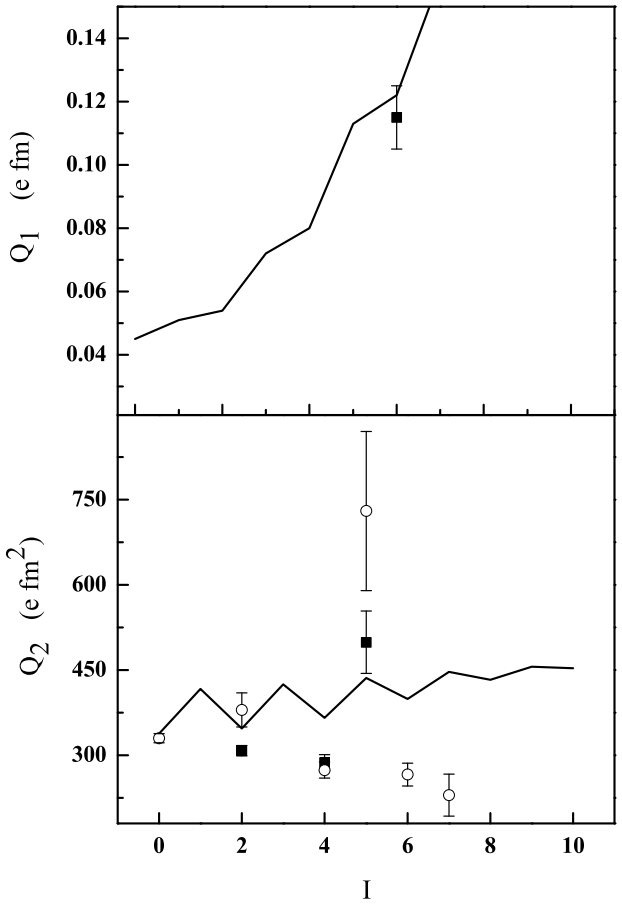

Fig. 4. Angular-momentum dependence of the calculated transitional electric dipole and quadrupole moments for ^{144}Ba (solid curve). The experimental data from this work are shown as squares and the weighted averages from previous publications, listed in tables 3 and 4, as open circles.

then the states of the positive parity have a smaller effective quadrupole deformation than the negative-parity states because the larger part of their wave functions is located near the barrier top compared to the wave functions of the negative-parity states. Being considered in the time-dependent picture the system is moving along the valley connecting a minimum with the barrier top (as seen in fig. 5 of [7]). This demonstrates the formation of the softer mode describing a motion in the $\beta_{20}\beta_{30}$-plane.

4 E2 transitions between negative-parity states in octupole vibrational nuclei

The cluster picture used in the previous section is compatible only with the situation when nuclei have octupole deformation or are near to be octupole deformed. In this case $E(1^-) < E(3^-)$. However, there are nuclei with low-lying negative-parity collective states and a rotational sequence of angular momenta of the excited states at higher I, *i.e.* $E(I^-) < E((I+1)^+) < E((I+2)^-) \ldots$, in which $E(1^-) > E(3^-)$. In this case we have at low I anharmonic octupole

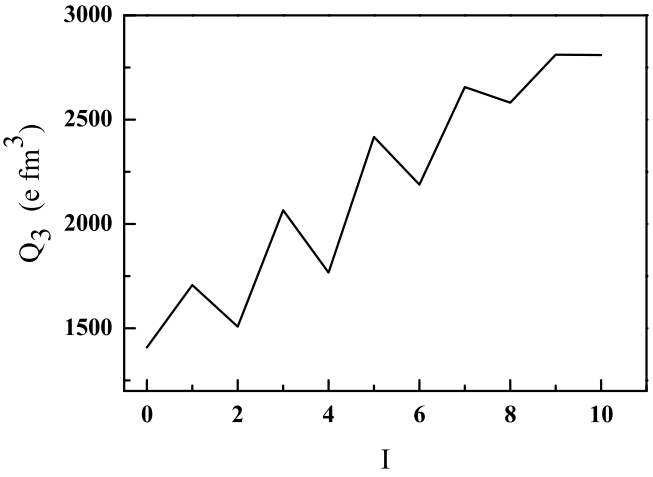

Fig. 5. Angular-momentum dependence of the calculated transitional electric octupole moment for ^{144}Ba (solid curve).

vibrations around $\beta_{30} = 0$ and the cluster degree of freedom η is insufficient to describe such collective motion. In this case both quadrupole β_{20} and octupole β_{30} degrees of freedom should be considered as independent ones.

To analyze the dependence on parity of the $E2$ transition probabilities $B(E2; (I+2)^\pi \to I^\pi)$ in these octupole vibrational nuclei let us consider a model which is a simplified version of the quadrupole-octupole coupling model formulated in [25,26].

We assume as in [25,26] that the quadrupole motion is characterized by the presence of a static quadrupole deformation which is large enough compared to the amplitude of the zero-point oscillations around equilibrium deformation. These oscillations are neglected in the Hamiltonian and the only degrees of freedom related to the quadrupole motion which are considered are rotational angles describing a rotation of the deformed quadrupole field. Concerning the octupole motion it is assumed that there are octupole vibrations around $\beta_3 = 0$ and there is also the quadrupole-octupole coupling term in the Hamiltonian. The Hamiltonian takes the form

$$H = H_{\rm core} + \hbar\omega_3 \sum_\mu f^+_{3\mu} f_{3\mu} + \kappa \sum_\mu (-1)^\mu Q^{(\rm quad)}_{2\mu} Q^{(\rm oct)}_{2-\mu}\,, \tag{9}$$

where κ is a parameter and $H_{\rm core}$ is a function of the angular momentum of the quadrupole mode R_μ,

$$H_{\rm core} = H_{\rm core}(\boldsymbol{R}^2)\,. \tag{10}$$

In the simplest case

$$H_{\rm core} = \frac{\hbar^2}{2\Im}\boldsymbol{R}^2. \tag{11}$$

The operator $f^+_{3\mu}(f_{3\mu})$ is the octupole boson creation (annihilation) operator. Since we neglect the quadrupole vibrations around equilibrium the operator $Q^{(\rm quad)}_{2\mu}$ is taken

to be equal to $\beta_2 D^2_{\mu 0}(\boldsymbol{\theta})$, and $Q^{(\mathrm{oct})}_{2\mu}$ is taken to be equal to

$$Q^{(\mathrm{oct})}_{2\mu} = \sum_{m,m'} C^{3m'}_{3m2\mu} f^+_{3m'} f_{3m}, \tag{12}$$

where $C^{3m'}_{3m2\mu}$ is the Clebsch-Gordan coefficient. The angular momentum of the quadrupole mode $\boldsymbol{R}$ acts only on the functions of the angle $\boldsymbol{\theta}$ and commutes with $f^+_{3\mu}$, $f_{3\mu}$.

The Hamiltonian (9) cannot be applied to description of nuclei with the strong octupole correlations like ^{144}Ba because of the harmonic approximation for the octupole motion expressed by the second term in (9). This Hamiltonian can be, in principle, diagonalized, however, it will require an introduction of the additional parameters which can vary significantly from one isotope to the other.

The octupole phonon operators commute with the Wigner function $D^2_{\mu 0}(\boldsymbol{\theta})$. Thus,

$$H = H_{\mathrm{core}} + \hbar\omega_3 \sum_\mu f^+_{3\mu} f_{3\mu} + \kappa\beta_2 \sum_\mu (-1)^\mu D^2_{\mu 0}(\boldsymbol{\theta}) \sum_{m,m'} C^{3m'}_{3m2\mu} f^+_{3m'} f_{3m}\,. \tag{13}$$

This Hamiltonian can be transformed into the intrinsic frame by the substitution

$$f^+_{3\mu} \to \sum_K D^3_{\mu K}(\boldsymbol{\theta}) b^+_{3K}\,, \qquad R_\mu \to I_\mu - j^{(\mathrm{oct})}_\mu\,, \tag{14}$$

where b^+_{3K}, b_{3K} are intrinsic boson operators,

$$[b_{3K}, b^+_{3K'}] = \delta_{KK'}\,, \tag{15}$$

I_μ is the total angular momentum operator whose action on the Wigner functions is determined by the standard relations

$$[I_\pm, D^I_{MK}] = \sqrt{(I \pm K)(I \mp K + 1)} D^I_{MK\mp 1}\,, \tag{16}$$

$$[I_0, D^I_{MK}] = K D^I_{MK}\,. \tag{17}$$

The intrinsic angular-momentum operator of the octupole mode $j^{(\mathrm{oct})}_\mu$ acts only on the octupole bosons b^+_{3K}, b_{3K}

$$[j^{(\mathrm{oct})}_\pm, b^+_{3K}] = \sqrt{(3 \mp K)(3 \pm K + 1)} b^+_{3K\mp 1}\,, \tag{18}$$

$$[j^{(\mathrm{oct})}_0, b^+_{3K}] = K b^+_{3K}\,. \tag{19}$$

The commutator $[R_\mu, f^+_{3\nu}]$, which is equal to zero, is transformed in the new variables to $[I_\mu - j^{(\mathrm{oct})}_\pm, \sum_K D^3_{\nu K} b^+_{3K}]$ and is equal to zero, as can be easily checked by straightforward calculations.

Thus, in the intrinsic frame the Hamiltonian (9) takes the form

$$H = H_{\mathrm{core}}\left((\boldsymbol{I} - \boldsymbol{j}^{(\mathrm{oct})})^2\right) + \sum_K \left(\hbar\omega_3 + \kappa\beta_2 C^{3K}_{3K20}\right) b^+_{3K} b_{3K}\,. \tag{20}$$

The eigenfunctions of this Hamiltonian for the lowest family of the positive-parity states are

$$\sqrt{\frac{2I+1}{8\pi^2}} D^I_{M0}|0\rangle\,, \tag{21}$$

where $|0\rangle$ is the vacuum state for intrinsic excitations. The eigenfunctions of the one-phonon negative-parity states are

$$\sqrt{\frac{2I+1}{8\pi^2}} \sum_K u^{(I)}_K D^I_{MK} b^+_{3K}|0\rangle\,, \tag{22}$$

where the coefficients $u^{(I)}_K$ are determined by diagonalization of the Coriolis term in the Hamiltonian (20). We do not need the concrete values of these coefficients for our further consideration and therefore assume only that they are smooth functions of I.

Let us calculate the reduced matrix elements of the $E2$ transition operator which in this model is given by the expression

$$Q_{2\mu} = \sqrt{\frac{5}{16\pi}} Q_{20} D^2_{\mu 0}\,, \tag{23}$$

where Q_{20} is the intrinsic quadrupole moment parameter. In the following, let I be an even number. Using (21) and (23) we obtain for transitions between positive-parity states,

$$\langle I \parallel Q_2 \parallel I-2\rangle = \sqrt{\frac{5}{16\pi}} Q_{20} \sqrt{2I-3} C^{I0}_{I-2020}\,. \tag{24}$$

For the transitions between negative-parity states we obtain, using (22) and (23),

$$\langle I+1 \parallel Q_2 \parallel I-1\rangle = \sqrt{\frac{5}{16\pi}} Q_{20} \sqrt{2I-1} \times \sum_K u^{(I+1)}_K u^{(I-1)}_K C^{I+1K}_{I-1K20}\,. \tag{25}$$

The last expression can be simplified using the following approximation for C^{IK}_{I-2K20}:

$$C^{IK}_{I-2K20} = \sqrt{\frac{3[(I-1)^2 - K^2][I^2 - K^2]}{(2I-3)(2I-2)(2I-1)I}} \approx \left(1 - \frac{K^2}{(I-1/2)^2}\right) C^{I0}_{I-2020}\,. \tag{26}$$

Substituting (26) in (25) we obtain

$$\langle I+1 \parallel Q_2 \parallel I-1\rangle = \sqrt{\frac{5}{16\pi}} Q_{20} \sqrt{2I-1} C^{I+10}_{I-1020} \times \left(1 - \frac{\sum_K K^2 u^{(I+1)}_K u^{(I-1)}_K}{(I+1/2)^2}\right)\,. \tag{27}$$

Assuming a smooth dependence of $u^{(I)}_K$ on I, we can write $\sum_K K^2 u^{(I+1)}_K u^{(I-1)}_K \approx \sum_K K^2 (u^{(I)}_K)^2 \equiv \langle I|K^2|I\rangle$.

Indeed, doing a Taylor expansion we obtain

$$\begin{aligned}
&\sum_K K^2 u_K^{(I+1)} u_K^{(I-1)} = \\
&= \sum_K K^2 \left(u_K^{(I)} + \frac{\mathrm{d}}{\mathrm{d}I} u_K^{(I)} + \frac{1}{2}\frac{\mathrm{d}^2}{\mathrm{d}I^2} u_K^{(I)} + \dots \right) \\
&\quad \times \left(u_K^{(I)} - \frac{\mathrm{d}}{\mathrm{d}I} u_K^{(I)} + \frac{1}{2}\frac{\mathrm{d}^2}{\mathrm{d}I^2} u_K^{(I)} + \dots \right) \\
&\approx \sum_K K^2 \left((u_K^{(I)})^2 + u_K^{(I)} \frac{\mathrm{d}^2}{\mathrm{d}I^2} u_K^{(I)} - \frac{\mathrm{d}}{\mathrm{d}I} u_K^{(I)} \cdot \frac{\mathrm{d}}{\mathrm{d}I} u_K^{(I)} \right) \\
&= \sum_K K^2 (u_K^{(I)})^2 \left(1 + \frac{\mathrm{d}}{\mathrm{d}I} \left(\frac{\frac{\mathrm{d}}{\mathrm{d}I} u_K^{(I)}}{u_K^{(I)}} \right) \right). \qquad (28)
\end{aligned}$$

The second term on the right-hand side of (28) contains the second-order derivative and the square of the first-order derivative of $u_K^{(I)}$ over I. We neglect this term following our assumption on a smooth dependence of $u_K^{(I)}$ on I.

Combining the results for $E2$ transitions between both positive and negative states we get

$$\begin{aligned}
\langle I \parallel Q_2 \parallel I-2 \rangle &= \sqrt{\frac{5}{16\pi}} Q_{20} \sqrt{2I-3} C^{I0}_{I-2020} \\
&\times \left(1 - \frac{1}{2}(1-(-1)^I) \frac{\langle I-1|K^2|I-1\rangle}{(I-1/2)^2} \right), \qquad (29)
\end{aligned}$$

where I can take both even and odd values. The last relation demonstrates the effect of staggering in the $E2$ reduced matrix elements and explains why in octupole vibrational nuclei like ^{148}Nd $E2$ transitions between negative-parity states are weaker than between positive-parity ones.

The values of $\sqrt{\langle I|K^2|I\rangle}$ which fit the experimental data [27,28] on $E2$ transition matrix elements $\langle I \parallel Q_2 \parallel I-2\rangle$ between the negative-parity states in ^{148}Nd are given in table 7. They are smaller than 3.0 in agreement with our assumption that the intrinsic excitations are the octupole vibrations. However, the value of $\sqrt{\langle K^2\rangle}$ needed to fit the experimental data for the $3^- \to 1^-$ transition is rather large. The experimental value of the $\langle 11^- \parallel Q_2 \parallel 13^-\rangle$ is significantly reduced compared to the rest of the band. This probably indicates a band crossing near $I^\pi = 13^-$.

Table 7. Values of $\sqrt{\langle I|K^2|I\rangle}$ extracted from the experimental data on the $E2$ reduced transition matrix elements, connecting negative-parity states in ^{148}Nd, using formula (29). The experimental data are taken from [28].

$I_\mathrm{i}^\pi \to I_\mathrm{f}^\pi$	$\sqrt{\langle \frac{1}{2}(I_\mathrm{i}+I_\mathrm{f})\|K^2\|\frac{1}{2}(I_\mathrm{i}+I_\mathrm{f})\rangle}$
$1^- \to 3^-$	2.2 ± 0.1
$3^- \to 5^-$	2.1 ± 0.1
$5^- \to 7^-$	2.8 ± 0.3
$7^- \to 9^-$	$0.8^{+1.1}_{-0.8}$
$9^- \to 11^-$	$2.1^{+1.0}_{-2.1}$

5 Conclusion

The experimental data on the $E2$ transition probabilities between the states of the ground-state alternating-parity bands of ^{144}Ba show a significantly larger value of the $E2$ transition probability between the negative-parity states compared to the positive-parity ones. This effect can be explained by a higher weight of the deformed component in the wave functions of the odd-I states. In the framework of the cluster approach it is explained by a higher weight of the alpha-cluster configuration, which is more deformed, in the wave function of the negative-parity states compared to the positive-parity ones. In the framework of the traditional collective model with the quadrupole and octupole degrees of freedom the effect of the increase of the $E2$ transition probability for the transitions between the negative-parity states is explained by a higher value of the quadrupole deformation at the minima of the potential energy as a function of β_{20} and β_{30} compared to its value at the top of the barrier separating two physically equivalent minima, having opposite signs of the octupole deformation. This picture is applied to nuclei which have permanent octupole deformation or are near to be octupole deformed such as ^{144}Ba.

The analysis of a dependence on parity of these $E2$ transition probabilities in the nuclei with the collective potential energy having minimum at $\beta_{30} = 0$ has shown that these nuclei are characterized by a nonzero average value of the projection of the intrinsic angular momentum of the octuple excitations on the intrinsic symmetry axis K. This decreases the $E2$ transition probabilities between the negative-parity states compared to the positive-parity ones which have $K = 0$. An example for such a situation is ^{148}Nd.

This work was supported in part by RFBR (Moscow), grant 04-02-17376 and BMBF grant 06MT190. R.V.J. thanks the Alexander von Humboldt Foundation for support.

References

1. I. Ahmad, P.A. Butler, Annu. Rev. Nucl. Part. Sci. **43**, 71 (1993).
2. P.A. Butler, W. Nazarewicz, Rev. Mod. Phys. **68**, 349 (1996).
3. R.V. Jolos, P. von Brentano, Phys. Rev. C **49**, R2301 (1994).
4. T.M. Shneidman, G.G. Adamian, N.V. Antonenko, R.V. Jolos, W. Scheid, Phys. Lett. B **526**, 322 (2002).
5. T.M. Shneidman, G.G. Adamian, N.V. Antonenko, R.V. Jolos, W. Scheid, Phys. Rev. C **67**, 014313 (2003).
6. F. Iachello, A.D. Jackson, Phys. Lett. B **108**, 151 (1982).
7. R.V. Jolos, Yu.V. Palchikov, V.V. Pashkevich, A.V. Unzhakova, Nuovo Cimento A **110**, 941 (1997).
8. R. Krücken *et al.*, in *Proceedings of the 11th International Symposium on Capture Gamma-Ray Spectroscopy and Related Topics - CGS11, Prague, Czech Republic, September 2002*, edited by J. Kvasil, P. Cejnar, M. Krticka (World Scientific, Singapore, 2003) p. 128.

9. D.C. Biswas *et al.*, Phys. Rev. C **71**, 011301 (2005).
10. T.M. Shneidman, G.G. Adamian, N.V. Antonenko, S.P. Ivanova, W. Scheid, Nucl. Phys. A **671**, 119 (2000).
11. R. Krücken, in *Proceedings of the International Symposium on Advances in Nuclear Physics, Bucharest, Romania, December 1999*, edited by D. Poenaru, S. Stoica (World Scientific, Singapore, 2000) p. 336.
12. I.Y. Lee, Nucl. Phys. A **520**, 641c (1990).
13. C. Hutter *et al.*, Phys. Rev. C **67**, 054315 (2003).
14. M. Cromaz, T.J.M. Symons, G.J. Lane, I.Y. Lee, R.W. MacLeod, Nucl. Instrum. Methods A **462**, 519 (2001).
15. A. Dewald, S. Harissopulos, P. von Brentano, Z. Phys. A **334**, 163 (1989).
16. W. Urban *et al.*, Nucl. Phys. A **613**, 107 (1997).
17. G.G. Adamian, N.V. Antonenko, R.V. Jolos, S.P. Ivanova, O.I. Melnikova, Int. J. Mod. Phys. E **5**, 191 (1996).
18. A.B. Migdal, *Theory of Finite Fermi Systems and Applications to Atomic Nuclei* (Wiley, NY, 1967).
19. G.G. Adamian, N.V. Antonenko, R.V. Jolos, Nucl. Phys. A **584**, 205 (1995).
20. J. Dudek, Prog. Part. Nucl. Phys. **28**, 131 (1992).
21. W.R. Phillips, I. Ahmad, H. Emling, R. Holzmann, R.V.F. Janssens, T.L. Khoo, M.W. Drigert, Phys. Rev. Lett. **57**, 3257 (1986).
22. S. Raman, C.W. Nestor jr., P. Tikkanen, At. Data Nucl. Data Table **78**, 1 (2001).
23. R. Krücken *et al.*, Phys. Rev. C **64**, 017305 (2001).
24. A. Bohr, B.R. Mottelson, *Nuclear Structure*, Vol. **2** (Benjamin, 1975).
25. M. Nomura, Phys. Lett. B **55**, 357 (1975).
26. D.R. Zolnowski, T. Kishimoto, Y. Gono, T.T. Sugihara, Phys. Lett. B **55**, 453 (1975).
27. R. Ibbotson *et al.*, Phys. Rev. Lett. **71**, 1990 (1993).
28. R.W. Ibbotson *et al.*, Nucl. Phys. A **619**, 213 (1997).